



OPEN

Design and biological evaluation of novel water-soluble complexes based on thiosemicarbazone as prospective anticancer agents

Sima Feizpour¹, Seyed Abolfazl Hosseini-Yazdi¹✉, Behzad Baradaran², Farhad Eslami³ & Elham Safarzadeh^{4,5}✉

The widespread success of platinum-based drugs in the clinical treatment of different neoplasia has led the inorganic metal complexes to be at the forefront of the fight against cancer. In this context, thiosemicarbazones and their metal derivatives serve as promising starting points for developing anticancer agents. In current study, the new fluorescent thiosemicarbazone ligand L and its complexes with some non-toxic first row transition metals such as Mn(II), Fe(III), Ni(II), Cu(II), and Zn(II) metal ions were attained as L^{Mn} , L^{Fe} , L^{Ni} , L^{Cu} , and L^{Zn} complexes. The molecular structures of the compounds were proved by chemico-physico techniques. The anti-proliferative activity of these compounds has been evaluated on human liposarcoma (SW-872) and human breast adenocarcinoma (MCF-7) using the MTT assay. The morphology of cell death and cell cycle studied in SW-872 cancerous cells was performed via flow cytometry. Eventually, imaging of treated cancerous cells with L^{Mn} and L^{Zn} complexes was performed by fluorescence microscopy. Compounds were designed in order to achieve a hydrophilic/lipophilic balance and synthesized through a condensation reaction. All compounds revealed high solubility in water and remained stable for more than 72 h in water as a neutral biological solvent. L^{Mn} and L^{Zn} complexes manifested good activity on SW-872 cancerous cells after 48 h exposure time (IC_{50} : $134.8 \pm 2.82 \mu\text{g/mL}$ and IC_{50} : $144.6 \pm 2.07 \mu\text{g/mL}$, respectively). The morphology of cell death in SW-872 cancerous cells treated with the L^{Zn} complex showed an apoptosis type cell death. Additionally, cell cycle studies declared the cell cycle arrest in the S phase for L^{Zn} . In conclusion, the development of water-soluble thiosemicarbazone complexes with intrinsic fluorescent properties promises to facilitate the detection of these compounds in living cells, aiding the investigation of their wide-ranging biological activities.

Keywords Cell cycle, Fluorescence microscopy, MCF-7, Thiosemicarbazone, SW-872

Thiosemicarbazones are an influential family of Schiff bases that have been considered for their ability to form complexes having pharmacological, biological, and analytical applications^{1–6}. Over the past few years, many thiosemicarbazones containing a variety of functional groups have been extensively studied to invent novel drug candidates⁷. The thiosemicarbazide moiety is a therapeutic key of a lot of anticancer thiosemicarbazone agents⁸. One of the most widely used thiosemicarbazone derivatives is 3-aminopyridine-2-carboxaldehyde thiosemicarbazone (trapiine) as a factor that has the inhibitory potential of ribonucleotide reductase, which has shown significant cytotoxic activity both in vitro and in vivo media^{9,10}.

Thiosemicarbazones comfortably construct stable metal complexes with different metal ions via their N and S atoms^{11–13}. According to many reports, metal complexes of thiosemicarbazones have considerably higher anti-proliferation activity than their corresponding ligands^{14,15}. The biological activity of thiosemicarbazones and their metal complexes is altered by modification of terminal nitrogen substitution. Diverse substitutive groups

¹Department of Inorganic Chemistry, Faculty of Chemistry, University of Tabriz, Tabriz 51666-14766, Iran.
²Immunology Research Center, Tabriz University of Medical Sciences, Tabriz 5166614731, Iran. ³Department of Biology, Faculty of Natural Sciences, University of Tabriz, Tabriz, Iran. ⁴Cancer Immunology and Immunotherapy Research Center, Ardabil University of Medical Sciences, Ardabil, Iran. ⁵Department of Microbiology, Parasitology and Immunology, Faculty of Medicine, School of Medicine, Ardabil University of Medical Sciences, Ardabil, Iran. ✉email: hosseiniyazdi@tabrizu.ac.ir; hosseiniyazdi@yahoo.com; Safarzadehelham@yahoo.com; Elham.im63@gmail.com

may cause different modes of activity and also provide additional features to inhibit the growth of human and animal tumors, viruses, fungi, and so on^{16–18}. Lipophilicity dominates the speed of moving molecules across cells, and it can be created by altering the thiosemicarbazone substitution. It also may be enhanced by being complexation^{19,20}. Therefore, thiosemicarbazones and their metal complexes have constantly attracted interest and have become promising research areas²¹.

Zinc is one of the most vital elements in biological systems that acts as a cofactor in many enzymes and is necessary for gene transcription, the transmission of nervous signals, and apoptosis^{22–24}. The connection between the deficit of zinc in alive organs and cancer has been considered by researchers whose purpose is the design of new metal-based drugs²⁵. Forever, plenty of zinc complexes have been prepared and evaluated as agents that have anticancer potential. By the way, studies of their anticancer mechanisms have revealed that zinc complexes can endanger the growth of cancer cells through the following methods: cell death by induction of cell apoptosis, targeting DNA, and other compounds in the nucleus^{26,27}.

Manganese is an essential element that forms the active site of several metalloproteins²⁸. Meanwhile, manganese is one of the most important biometals due to its presence in the active centers of numerous enzymes and its various functions. Teslascan and SC-52608 are the most well-known manganese compounds used in MRI and as an anticancer agent in medicine, respectively. In the field of inorganic biochemistry, the bioactive potential of manganese compounds has been considered by researchers. According to reported articles, manganese compounds have shown promising anticancer, antimicrobial, antifungal, and antioxidant activity^{29,30}.

Previously in our research group, thiosemicarbazone derivatives containing sulfonate substituent and their complexes have been synthesized, which displayed good solubility and stability in water, antibacterial, antifungal, and antioxidant activity^{31–34}. In this project, a novel fluorescent ligand with accompanying sulfonate substituent and some of its metal complexes were synthesized. These compounds were evaluated for stability and solubility in water. Meanwhile, the synthesized compounds have fluorescent emissions that can be used to image cancer cells.

Material and methods

Chemicals and instrumentation

All chemicals, solvents, and biological materials were obtained from commercial sources and these materials were utilized without purification. 4-(1-naphthyl)-3-thiosemicarbazide was synthesized according to the multi-step protocol based on previous researches^{35–39}. Also, sodium salicylaldehyde-5-sulfonate hydrate was prepared according to the prior publication by our research group³¹. FT-IR spectrometer Bruker Tensor 27 recorded FT-IR spectra of synthesized compounds using a KBr disk in 4000–400 cm^{–1}. The ligand (L) and its Zn(II) complex (L^{Zn}) were characterized by ¹H NMR spectroscopy. Their spectra were acquired on a Bruker Avance 400 spectrometer in DMSO-*d*₆ as a solvent and residual solvent as standard. Absorption electronic spectra were measured on a Shimadzu UV-Vis 1700 spectrophotometer in an aqueous solution of the compounds over the wavelength range 230–1100 nm. Molar conductivity of the compounds' was recorded by a Cond 7110 WTW conductometer. A EuroVector Elemental Analyzer EA3000 was used to determine Elemental analysis data (C, H, N, S). All studied cell lines were prepared from the National Cell Bank of Iran (Pasteur Institute, Tehran, Iran). The absorption value of formazan dye of MTT assay was measured by BioTek Synergy HT microplate reader (BioTek Instruments Inc., USA). In order to flow cytometry studies, the Partec CyFlow Space flow cytometer was used, and the obtained results were analyzed using FlowJoTM V10.0 Software (BD Life Science). The fluorescence spectra were collected on a JASCO FP-750 model spectrofluorimeter. The images of treated MCF-7 cells with synthesized fluorescent compounds were taken by Cyvation 5 Imaging Multi-Mode Reader fluorescence microscope.

Preparation of the ligand (L) and its complexes

Synthesis of sodium-4-hydroxy-3-((2-(naphthalene-1-ylcarbamothioyl)hydrazono) methyl)benzenesulfonate (NaH₂LSO₃·1.5H₂O, L)

(10 mmol, 2.17 g) of 4-(1-naphthyl)-3-thiosemicarbazide was dissolved in 80 mL of methanol. After that, a methanolic solution of sodium salicylaldehyde-5-sulfonate hydrate (10 mmol, 2.27 g) was added dropwise to the content of reaction mixture. The mixture was stirred for 3 h at room temperature. The yellowish precipitate of the ligand (L) was obtained after slow evaporation of the reaction solution at room temperature. The product was filtered and dried in ambient conditions. Yield: 2.92 g (65%); Color: Yellowish; Anal. Calc. (%) for C₁₈H₁₇N₃NaO_{5.5}S₂, NaH₂LSO₃·1.5H₂O (F.W = 450.46 g/mol); C: 47.99, H: 3.80, N: 9.33, S: 14.24, found (%); C: 47.96, H: 3.68, N: 8.75, S: 13.97. Selected FT-IR data (KBr, cm^{–1}): 3435m, 2929w, 2852w, 1609s, 1515s, 1396, 1323, 1197s, 1110s, 1037s, 945, 833s, 769s, 664s, 600s. ¹H NMR (δ , ppm, DMSO-*d*₆): 6.89 (1H, d, ArH_{ph}), 7.54–7.57 (5H, m, ArH_{naph}), 7.90 (2H, t, ArH_{naph}), 7.98 (1H, d, ArH_{ph}), 8.24 (1H, s, ArH_{ph}), 8.59 (1H, s, CHN), 10.21 (1H, broad s, NH), 10.44 (1H, s, NH), 11.88 (1H, s, OH).

Synthesis of the complexes

Public protocol: the metal chloride salts were dissolved in methanol solvent and added to a methanolic solution of L gradually. The mixture of reactants was stirred for 3 h. The solvent was reduced under slow evaporation at room temperature. Finally, the complexes have appeared as sediment.

(L^{Mn}): Through the mentioned protocol, L^{Mn} was obtained from MnCl₂·2H₂O (2 mmol, 0.34 g) and L (1 mmol, 0.45 g). Yield: 0.43 g (64%); Color: yellowish; Anal. Calc. (%) for C₁₈H₂₃Cl₂Mn₂N₃NaO₅S₂, Mn₂(HL)Cl₂·5H₂O (F.W = 670.30 g/mol); C: 32.25, H: 3.46, N: 6.27, S: 9.57, found (%); C: 32.55, H: 3.26, N: 5.83, S: 9.48. Selected FT-IR data (KBr, cm^{–1}): 3435m, 2958m, 1623s, 1521s, 1165s, 1030s, 775s, 633s, 591s.

(L^{Fe}): The intended complex was synthesized by FeCl₃ (1 mmol, 0.16 g) and L (1 mmol, 0.45 g). Yield: 0.42 g (81%); Color: dark brown; Anal. Calc. (%) for C₃₆H₃₂Cl₂Fe₂N₆O₁₁S₄, Fe₂(HL)₂Cl₂·3H₂O (F.W = 1035.52 g/mol);

C: 41.75, H: 3.11, N: 8.12, S: 12.39, found (%); C: 42.10, H: 3.09, N: 7.46, S: 12.39. Selected FT-IR data (KBr, cm^{-1}): 3383m, 3057w, 2944w, 1597s, 1491m, 1419s, 1301m, 1161s, 1110m, 1026s, 770s, 667s, 587s.

(L^{Ni}): This complex was achieved from $\text{NiCl}_2 \cdot 6\text{H}_2\text{O}$ (1 mmol, 0.24 g) and L (1 mmol, 0.45 g). Yield: 0.39 g (81%); Color: light green; Anal. Calc. (%) for $\text{C}_{36}\text{H}_{31}\text{N}_6\text{Ni}_2\text{O}_{10.5}\text{S}_4$; $\text{Ni}_2(\text{HL})_2 \cdot 2.5\text{H}_2\text{O}$ (F.W = 961.32 g/mol); C: 44.98, H: 3.25, N: 8.74, S: 13.34, found (%); C: 45.35, H: 3.58, N: 8.33, S: 13.21. Selected FT-IR data (KBr, cm^{-1}): 3429m, 3191w, 2978w, 1604s, 1549s, 1423s, 1346m, 1277m, 1219s, 1151s, 1026s, 948m, 775s, 664s, 593s, 529m.

(L^{Cu}): This complex was prepared by $\text{CuCl}_2 \cdot 2\text{H}_2\text{O}$ (1 mmol, 0.17 g) and L (1 mmol, 0.45 g). Yield: 0.35 g (76%); color: green; Anal. Calc. (%) for $\text{C}_{36}\text{H}_{26}\text{N}_6\text{Cu}_2\text{O}_8\text{S}_4$; $\text{Cu}_2(\text{HL})_2$ (F.W = 925.98 g/mol); C: 46.69, H: 2.83, N: 9.08, S: 13.85, found (%); C: 46.88, H: 3.40, N: 5.56, S: 13.86. Selected FT-IR data (KBr, cm^{-1}): 3430s, 2921w, 1630s, 1424w, 1374m, 1299w, 1175m, 1108m, 1024s, 802s, 669s, 588s.

(L^{Zn}): By a similar method, L^{Zn} was earned from ZnCl_2 (1 mmol, 0.14 g) and L (1 mmol, 0.45 g). Yield: 0.34 g (68%); color: yellow; Anal. Calc. (%) for $\text{C}_{36}\text{H}_{28}\text{Cl}_2\text{N}_6\text{O}_8\text{S}_4\text{Zn}_2$; $\text{Zn}_2(\text{H}_2\text{L})_2\text{Cl}_2$ (F.W = 1000.61 g/mol); C: 43.21, H: 2.62, N: 8.40, S: 12.82, found (%); C: 42.93, H: 2.61, N: 8.41, S: 13.05. Selected FT-IR data (KBr, cm^{-1}): 3437m, 3193m, 2999w, 1613w, 1541s, 1468s, 1292m, 1231w, 1140s, 1022s, 779m, 671m, 592s. ^1H NMR (δ , ppm, DMSO- d_6): 6.87 (1H, d, ArH_{ph}), 7.52–7.56 (5H, m, ArH_{naph}), 7.88–7.89 (2H, m, ArH_{naph}), 7.97 (1H, d, ArH_{ph}), 8.22 (1H, s, ArH_{ph}), 8.56 (1H, s, CHN), 10.19 (1H, s, NH), 10.42 (1H, s, NH), 11.85 (1H, s, OH).

Measurement of lipophilicity

In order to estimate the lipophilicity of the compounds, the shake-flask method was used. 3 mL aqueous solution containing a certain concentration of each compound was stirred at room temperature for 24 h with 3 mL of 1-octanol. The solution was centrifuged to separate two phases from each other. Using spectrophotometry, the concentration of all compounds in the aqueous phase before and after blending with 1-octanol was measured ($D = [\text{Sample}]_{\text{org}} / [\text{Sample}]_{\text{aq}}$).

Fluorescence measurements

The fluorescence emission spectra of L and its complexes were obtained at room temperature by JASCO FP-750 spectrofluorometer. The solution of the mentioned compounds was prepared with HPLC grade water. The quantum efficiencies of the compounds (Φ_F) were defined by comparison with the integrated emission spectrum of standard quinine in 0.1 M H_2SO_4 solution at 360 nm as an excitation wavelength ($\Phi_F = 0.54$). Quantum efficiency is estimated by the following equation:

$$\varnothing_x = \varnothing_s \left(\frac{F_x}{F_s} \right) \left(\frac{A_s}{A_x} \right) \left(\frac{n_x}{n_s} \right)^2$$

\varnothing_x and \varnothing_s are known for the sample and standard radiative quantum efficiency, F_x and F_s are the integrated emission intensity of the spectrum for the sample and standard between 380–700 nm, A_x and A_s are the sample and standard absorptions at 360 nm as an excitation wavelength, and n_x and n_s are sample and standard solution reflection index.

Biological studies

Cell lines and culture conditions

In the current study, two cancerous cell lines including human breast adenocarcinoma (MCF-7) and human liposarcoma (SW-872) were selected to evaluate the anticancer ability of the prepared compounds. As a normal control, we chose human fibroblast cells (HFF-2). MCF-7, SW-872, and HFF-2 cell lines were prepared from the National Cell Bank of Iran (Pasteur Institute, Tehran, Iran). All cells were grown in 25 cm^2 cell culture flasks using RPMI (Roswell Park Memorial Institute) 1640 medium with phenol red (Biosera) supplemented with 10% (V/V) fetal bovine serum (FBS, Gibco) and 1% penicillin (1000 u/mL)/streptomycin (10 mg/mL) (Gibco) and were kept in a cell incubator at 37 °C, 5% CO_2 , and humidified conditions. When the cultures attained 80–90% confluence, cells were subcultured to ensure proper growth and health.

Cell viability assay

Colorimetric microculture assay (MTT assay) was used to determine the cytotoxicity of the mentioned compounds. The density of 1.2×10^4 cells/well was seeded on 96 well plates for in vitro studies of the anti-proliferation effect of synthesized compounds. After 24 h or more, when cells resumed their exponential growth, the cells were treated with 7 different concentrations of each compound (25–200 $\mu\text{g}/\text{mL}$ for L^{Mn} and 50–400 $\mu\text{g}/\text{mL}$ for other compounds). After spending the prescribed time of treatment, the belonging media to each well, including compounds, was replaced with 100 μL of fresh RPMI containing 10% FBS and 50 μL of 2 mg/mL MTT (3-(4,5-dimethylthiazol-2-yl)-2,5-diphenyltetrazolium bromide) (Sigma) and the plates were incubated again for 4 h. Once more, the media was removed and 200 μL DMSO was added to each well, and the plates were incubated for 30 min. The amount of formazan dye adsorption per well at 570 nm was measured by a BioTek Synergy HT microplate reader (BioTek Instruments Inc., USA). All tests for each concentration were done as duplicates. Cisplatin and Paclitaxel were considered as positive control drugs against cancer cells. IC_{50} values for each compound were calculated by Graph-Pad Prism software.

Apoptosis determination by Annexin V-FITC/PI assay

The apoptosis induction of L^{Zn} complex on the SW-872 cell line was investigated by the flow cytometry method using the annexin V-FITC/PI staining based on the Detection Kit procedure (eBiosciences kit). The cells (2×10^5 cells per well) were seeded in 6 well plates and after 48 h incubation in a cell culture incubator, they were exposed to IC_{25} concentration of the mentioned substance for 18 h. The culture medium of each well was emptied and

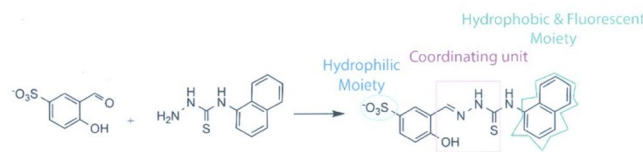


Fig. 1. Synthesis pathway of **L**.

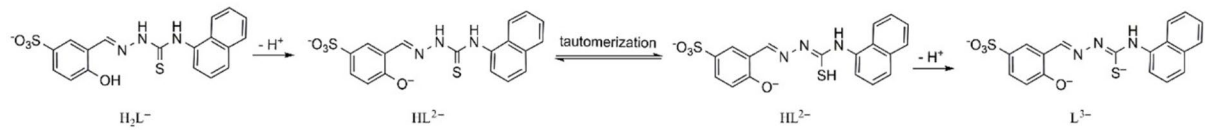


Fig. 2. The possible various species of the ligand (**L**).

the cells were harvested by trypsinization. Then, the cells were washed twice with PBS and the contents of each well were dispersed in 500 μ L of binding buffer. After that, the cells were stained with 5 μ L of annexin V-FITC and incubated for 15 min in the dark place at room temperature. The cells were washed with binding buffer and resuspended in 500 μ L of binding buffer. In the last step, 5 μ L of PI was added to the contents of each well and incubated for 10 min under normal conditions. The cells were assayed by a flow cytometer (Partec CyFlow space), and the data were analyzed with FlowJo™ V10.0 Software (BD Life Science).

Cell cycle arrest

SW-872 cells were plated at a density of 2×10^5 cells per well in a 6 well plate and then incubated for 24 h or more under the mentioned conditions. The cells were treated with an IC_{25} concentration of L^{Zn} complex and kept for 18 h in the cell culture incubator. Therefore, the cells were separated by trypsinization and were washed twice using cold PBS. The cells were put on ice for 10 min. The cells belonging to each well were stained by 250 μ L of a solution containing 10 μ g/mL DAPI and they were incubated at room temperature and darkness for 15 min. Next, the content of DNA was measured by a flow cytometer UV section and FL4 channel.

Imaging by fluorescent feature

For this purpose, human breast cancer cells (MCF-7) were distributed in a 6 well plate and placed in a humidified incubator at 37 °C and 5% CO₂ for 24 h or more. After that, the cells were treated with an aqueous solution with 10 and 100 μ M concentrations of L^{Mn} and L^{Zn} complexes for 1 and 4 h. After the treatment duration, the cells were washed with PBS and they were imaged using a fluorescence microscope.

Results and discussion

Design and synthesis

According to Fig. 1, the synthesized ligand (**L**) consists of three parts: the first part is made up of a hydrophobic component that facilitates the molecule's entrance into the hydrophobic environment of proteins. For this purpose, a naphthyl group was selected, which while having the hydrophobicity feature, this part has significant fluorescence emission. The second part includes the thiosemicarbazone moiety, which has inherently lone pair electrons that can coordinate to metal cations. The third part is a sulfonated section that leads to easy solubility in aqueous media and has biological activity in the aqueous medium of intracellular.

L was obtained after a condensation reaction between sodium salicylaldehyde-5-sulfonate and 4-(1-naphthyl)-3-thiosemicarbazide in methanol solvent with a 1:1 molar ratio according to Fig. 1^{31,32}.

The ligand shows good solubility in water, 4.42 g/L. As well as, **L** is soluble in polar solvents like DMSO, DMF, MeOH, and EtOH. This ligand (**L**) dissolves less in water than other synthesized derivatives³¹⁻³³. In the FT-IR spectrum of **L**, the absorption band belonging to the stretching vibration of the imine group (C = N) has appeared at 1609 cm^{-1} , which acts as evidence for the synthesis of the desired Schiff-base ligand. In addition, based on ¹H NMR spectra ascribed to **L**, the singlet peak belonging to imine hydrogen (CHN) has been observed at 8.59 ppm, which is further evidence for the formation of Schiff-base ligand. All hydrogens were referred to their respective peaks and no additional peaks were observed in the ¹H NMR spectra, which indicates the high purity of the reaction product (**L**) (Fig S1). Phenolic proton and protons on the nitrogen atoms were assigned by adding some drops of D₂O to DMSO-*d*₆ solution. Signals at 11.88, 10.44, and 10.21 ppm start to diminish after D₂O addition (Fig S2).

The various species of the ligand that can be present and be coordinated to the central metal ions are exhibited in Fig. 2. The thione-phenol H_2L^{-} thione-phenol species can be converted to thione-phenolate form HL^{2-} thione-phenolate species by pH increasing. This species can be tautomerized to HL^{2-} thiol-phenolate form. The other possible species is L^{3-} thiolate-phenolate as the thiolate-phenolate type that can be existed in high pHs.

Comparison FT-IR spectra of complexes with free ligand provides useful information on the coordination of ligand to the central metal (Figs S5-S10). A strong absorption band attributed to the stretching vibration of

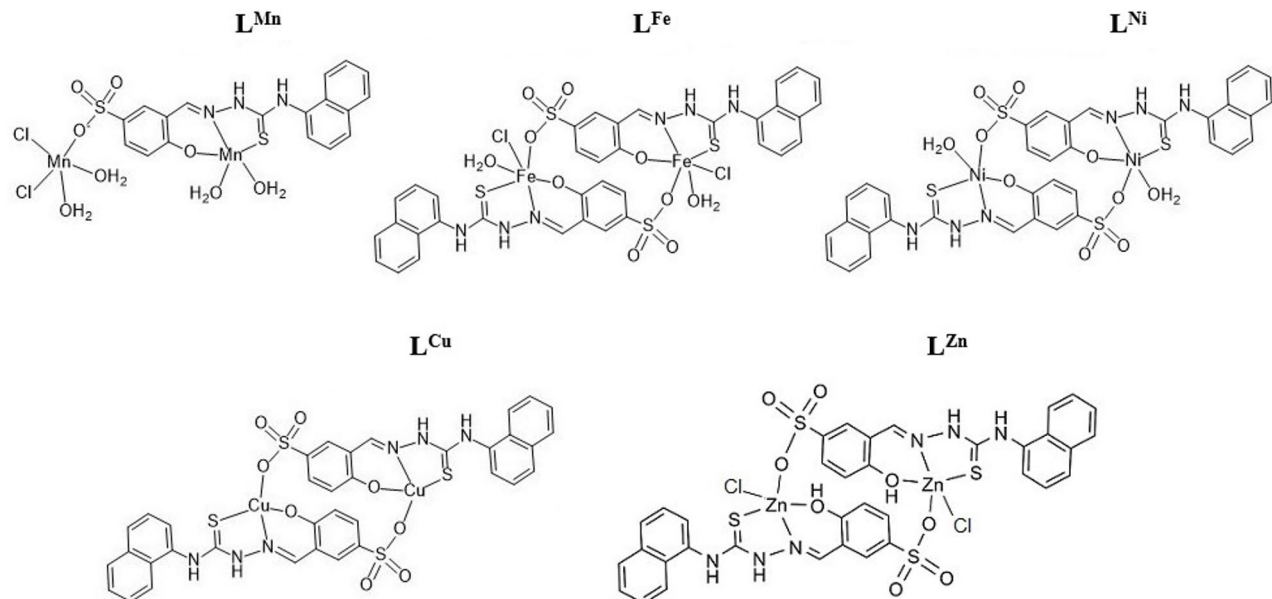


Fig. 3. Proposed structures for the complexes prepared by ligand L.

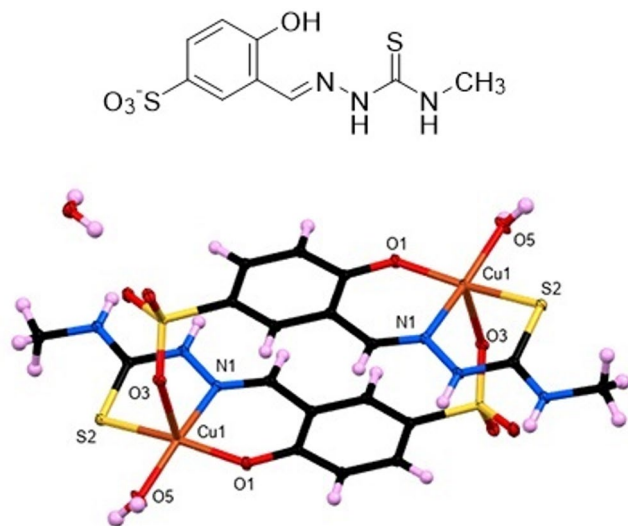


Fig. 4. Structure of the 4-hydroxy-3-((methylaminocarbonothioyl)hydrazone) methylbenzenesulfonate and molecular structure of copper(II) complex.

the imine group ($C=N$) for free ligand appears at 1609 cm^{-1} , while corresponding absorption band of $C=N$ for complexes appeared at different wavenumbers in comparison with the free ligand. This could be a verification of the claim that the iminic nitrogen of the ligand is coordinated to the metal center in the solid state.

Based on the obtained data from elemental analysis, the ratio of ligand to metal in all complexes except the Mn(II) complex is 1:1. According to the electronic absorption spectrum of L^{Mn} no signal has appeared in the visible range, which corresponds to the d_{hs}^5 electronic configuration in a weak field. A binuclear structure is assigned for the mentioned complex so that L is coordinated to the central metal through NSO donors, also the ligand is coordinated via its sulfonate side to another metal cation. Therefore, H_2O molecules and chloride ions are placed in other vacant positions (Fig. 3). Based on the results of single crystal X-ray crystallography of previously synthesized complexes related to this family of ligands (Fig. 4)^{31–33}, it can be predicted that the L^{Fe} complex is a dinuclear in the solid state. The geometry around Fe(III) metal cation is octahedral, which is located H_2O molecule and a chloride ion in 5 and 6 positions. Two oxygen of two sulfonates functional group assigned to two separate ligands occupy the optical position on both metal centers and act as a bridge between them. The attained value for molar conductivity also confirms the release of ions in the aqueous solution of

this complex (Table 1). The absorption electronic spectrum of the mentioned complex unfolds a strong broad band in the visible region, which is a feature of d_{ls}^5 electron configuration in the presence of a strong octahedral field. A dimeric form is also predicted for the L^{Ni} , L^{Cu} , and L^{Zn} complexes, as the two ligands in the structure of each complex act as a bridge between two metal centers through the oxygen of the sulfonate group. In the L^{Ni} complex, there are H_2O molecules in the empty positions. In the absorption electronic spectrum of L^{Ni} , it was also observed a broad peak specific to the octahedral field at the visible region. In the absorption electronic spectrum, the visible area of L^{Cu} corresponds to the d-d transition of the d^9 configuration with the square planar field. In L^{Mn} , L^{Fe} , L^{Ni} , and L^{Cu} complexes, the ligand is tridentately coordinated to the central metal cation through SNO donor atoms and in the HSO_3^{2-} thione-phenolate form. According to the 1H NMR spectrum related to the L^{Zn} complex, it can be proved that the ligand is introduced to H_2L^{Zn} thione-phenol form in the structure of the complex after coordination. The signal of OH group in $DMSO-d_6$ for L^{Zn} observes at 11.85 ppm which starts to disappear after addition of some drops of D_2O (Figs S3, S4). The molar conductivity values also show the presence of free ions in the aqueous solution of this complex. According to this evidence, it confirms that coordinated anions in the solid state (Fig. 3) dissociate in water. The ESI-MS spectra of the ligand and its complexes in methanol solution are shown in Figs S11-S16.

In previous research work carried out in 2017 by our research group³³, the water-soluble ligand: sodium 4-hydroxy-3-(([(methylaminocarbonothioyl)hydrazono]methyl)benzene sulfonate and nickel(II), copper(II), and zinc(II) complexes are also prepared from this ligand. Based on the crystallographic data for the copper complex, the binuclear structure has been confirmed in the solid state (Fig. 4). While mass spectrometry investigation of the copper complex showed that this complex is mononuclear in methanolic or aqueous solution due to the competition of the coordinating solvents to occupy the coordination positions. Based on the results of the elemental analysis of the complexes (CHNS) and previous experiences, all of the complexes are dinuclear only in the solid state while in water solution the complexes are converted to mononuclear species.

Stability and solubility

The solubility of the compounds L , L^{Mn} , L^{Fe} , L^{Ni} , L^{Cu} , and L^{Zn} in water are 4.4, 3.2, 2.5, 1.4, 1.6, and 2.4 g/L, respectively. In addition, these compounds dissolve well in solvents such as DMSO, DMF, MeOH, and EtOH. The stability of the synthesized ligand L and its complexes in an aqueous solution (physiological conditions with pH 7.3, prepared by Tris buffer) under different time intervals, 0, 24, 48, and 72 h after preparation, was examined by UV-Vis spectroscopy (Fig. 5). No considerable variations were seen between the absorption electronic spectra of 24, 48, and 72 h after preparation compared to the UV spectra of the freshly prepared aqueous solution. Therefore, the compounds showed good stability in a neutral aqueous solution.

Absorption and emission spectra of the compounds

The absorption and emission spectra of the ligand and its complexes had been reported in Figs. 6 and 7, respectively, and the obtained results had been summarized in Table 1. The absorption bands that have appeared in the range of 230–430 nm are assigned to $\pi-\pi$ and $n-\pi^*$ transitions for naphthyl and phenyl rings and the azomethine group which it is difficult to identify accurately. The spectral pattern in the ultraviolet region of all compounds follows a similar trend due to the presence of the same chromophore in their structure. Although, $Fe(III)$, $Ni(II)$, and $Cu(II)$ complexes manifested a broad band in the visible region due to their d-d transitions. The excitation wavelength in the fluorescence spectra of compounds was selected 360 nm. The quantum efficiencies for the compounds earned compared to quinine sulfate as a standard. The emission spectra related to the L , L^{Mn} , L^{Ni} , and L^{Zn} compounds show an almost identical pattern with a maximum about 490 nm, while the spectral patterns of L^{Fe} and L^{Cu} are different from them, and their maximum is obvious at 437 and 470 nm, respectively.

Lipophilicity

Lipophilicity is a significant physicochemical feature of the medicine panorama. This feature controls the biological behavior of drugs, like membrane transferring and interaction with biological receptors. Accordingly, the detected correlation between lipophilicity and the biological activity of the drug is generally a related characteristic that should be checked^{40,41}. The lipophilicity of the compounds has been investigated using the shake flask method and the distribution coefficient (D) between the aqueous and 1-octanol phases has been calculated for each compound which was attained in the range of 4.9–97.3 (Table 1).

Compounds	λ_{max} (nm)	ϵ ($M^{-1}cm^{-1}$)	C (M)	λ_{ex} nm	Φ_F	Λ_m ($\Omega^{-1}cm^2mol^{-1}$)	D
L	290, 330	89750, 73223	1.12×10^{-5}	360	1.9×10^{-3}	96	4.9
L^{Mn}	280	51868	1.21×10^{-5}	360	4.9×10^{-3}	258	18.7
L^{Fe}	295	71753	1.70×10^{-5}	360	4.2×10^{-3}	393	73.3
L^{Ni}	370	40471	1.72×10^{-5}	360	0.3×10^{-3}	46	49.2
L^{Cu}	405	80871	1.79×10^{-5}	360	0.6×10^{-3}	43	97.3
L^{Zn}	295, 365	35209, 50302	1.72×10^{-5}	360	1.4×10^{-3}	353	6.4

Table 1. Summarized data for absorption and emission spectra, molar conductivity (Λ_m), and distribution coefficient (D) for all compounds. C: Concentration of compounds based on M (mol/L).

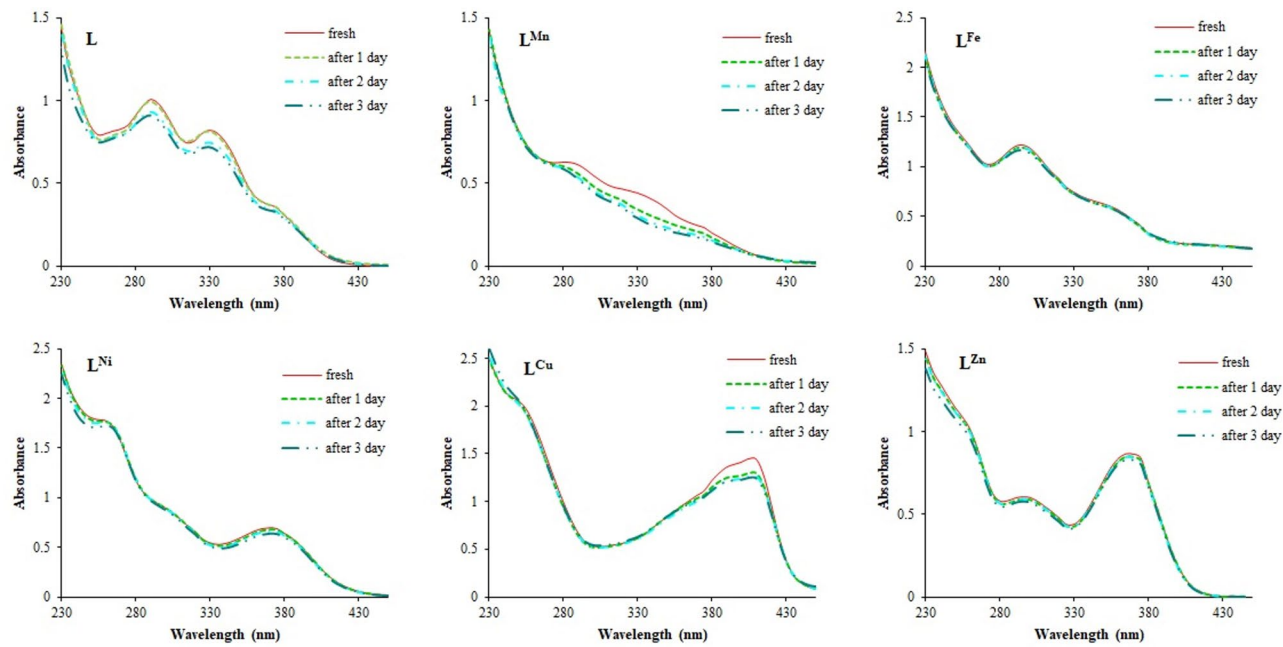


Fig. 5. Evaluation of UV-Vis spectra alteration in Tris buffer solution, pH 7.3, under different intervals time 0, 24, 48, and 72 h after preparation for **L** and its complexes.

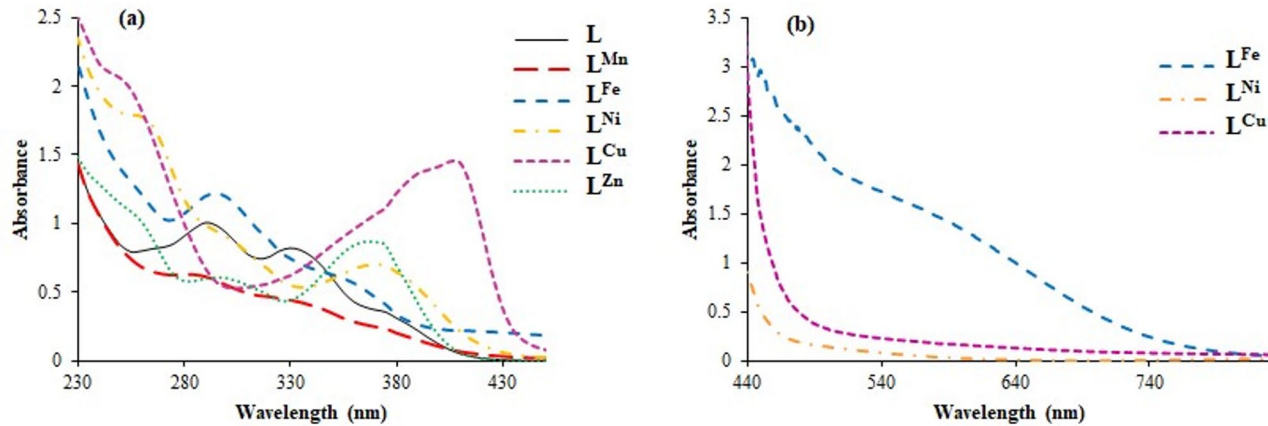


Fig. 6. UV-Vis spectra of the **L** and its complexes; (a): UV, (b): Visible.

Biological section

In vitro cytotoxicity studies by MTT assay

The capability of the ligand and its attributed complexes to inhibit the cancerous cells' growth in vitro against two cancer cell lines MCF-7 and SW-872, and a normal cell line HFF-2 was assessed by the MTT colorimetric assay. The obtained IC_{50} values for the ligand and its complexes are given in Table 2. IC_{50} values for L^{Mn} and L^{Zn} complexes against SW-872 cells were $268.9 \pm 3.38 \mu\text{g/mL}$ and $169.4 \pm 2.23 \mu\text{g/mL}$, respectively after 24 h treatment that remarkably lower than the parent ligand and this result is gained that predominantly the formation of metal complexes increases anti-proliferative activity against the SW-872 cancer cells (Fig. 8). Given the significant anti-proliferative effect of L^{Zn} , this compound was selected for further study.

Synthetic compounds displayed less toxicity against HFF-2 as normal cells in comparison with PTX (paclitaxel) and cisplatin, as commercial drugs. The anti-proliferative activity of the compounds was directly depended on the duration of cell treatment and increasing the treatment time due to an increase in toxicity and growth inhibition. Evaluation of toxicity effect related to compounds against MCF-7 cancer cell line revealed $IC_{50} > 800 \mu\text{g/mL}$ which can concluded that the synthesized compounds have performed better against the SW-872 cell line.

The enhanced cytotoxic activity of the complexes compared to the parent ligand can be explained by chelation theory. In these complexes, the positive charge of the metal center is shared with the ligand donor atoms and

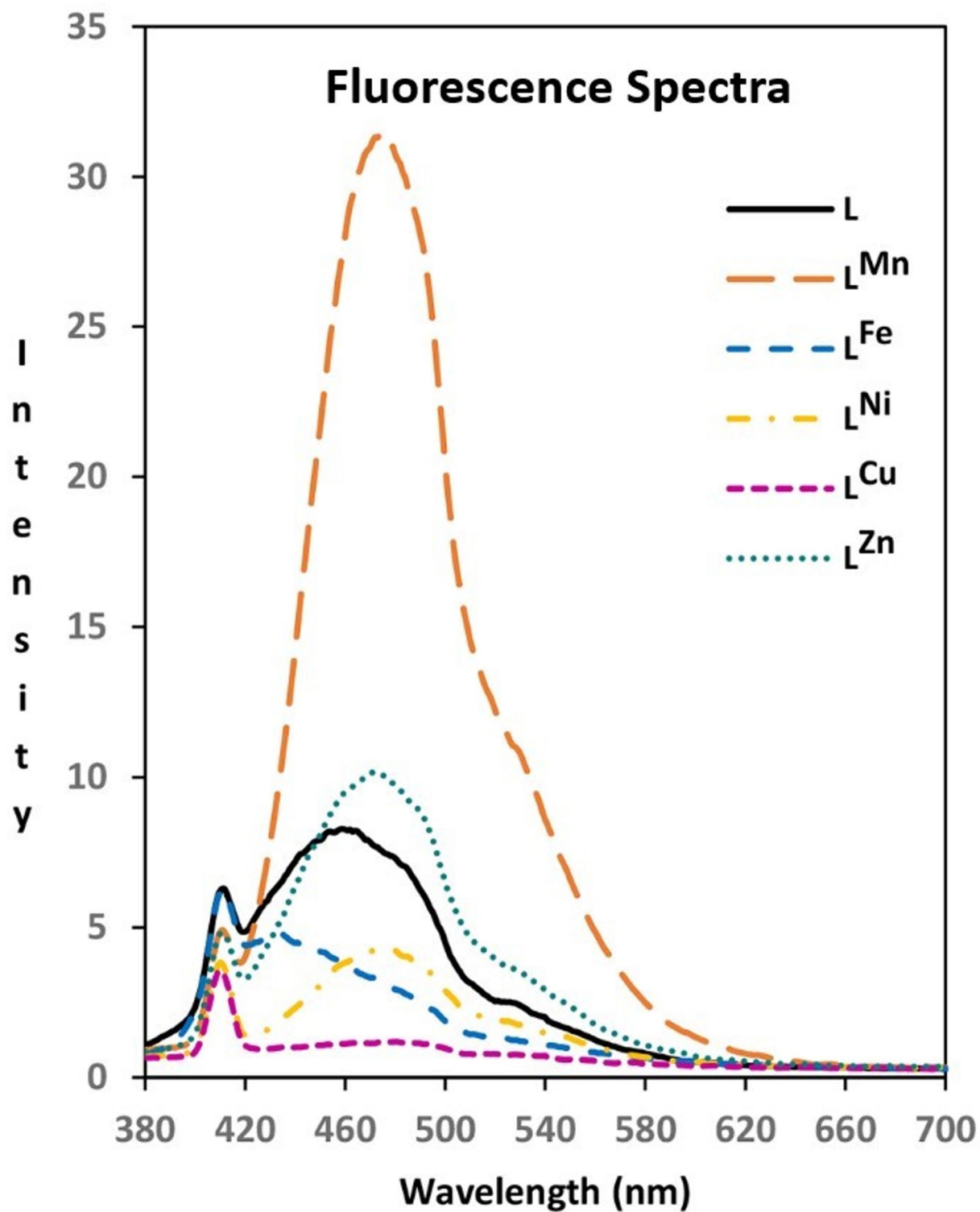


Fig. 7. The emission spectra of the ligand and its related complexes ($\lambda_{\text{ex}} = 360 \text{ nm}$).

there is a π -electron transfer across the chelate system. Chelating leads increase in the lipophilicity of the complexes, making it easier for the complex to penetrate the lipid layer of the cell membrane. Other factors, such as increased solubility, conductivity, coordination state, and the metal-ligand bond length, also contribute to the cytotoxic activity. Additionally, different efficacy levels are observed in various cell lines. In addition, transition metals like zinc, manganese, and copper can interact with the active sites of enzymes and play a significant role in biological activity. The ability of these complexes to bind and cleave DNA has been identified as a mechanism of metal complex-mediated cytotoxicity. Therefore, these complexes not only demonstrate greater activity but also

compounds	IC ₅₀ (μg/mL)					
	MCF-7		SW-872		HFF-2	
	24 h	48 h	24 h	48 h	24 h	48 h
L	>800	>800	>500	>500	>1000	>1000
L ^{Mn}	>800	>800	268.9 ± 3.38 (401.2 ± 5.04 μM)	134.8 ± 2.82 (201.1 ± 4.21 μM)	197.8 ± 2.28 (295.1 ± 3.40 μM)	186.5 ± 2.34 (278.2 ± 3.49 μM)
L ^{Fe}	>800	>800	>500	>500	>1000	>1000
L ^{Ni}	>800	>800	>500	>500	>1000	>1000
L ^{Cu}	>800	>800	>500	>500	>1000	>1000
L ^{Zn}	>800	>800	169.4 ± 2.23 (169.3 ± 2.22 μM)	144.6 ± 2.07 (144.5 ± 2.06 μM)	88.91 ± 2.43 (88.85 ± 2.42 μM)	72.05 ± 1.72 (72.00 ± 1.71 μM)
Paclitaxel	65.21 ± 1.15 (76.37 ± 1.35 μM)	22.32 ± 1.42 (26.14 ± 1.66 μM)	3.11 ± 1.46 (3.64 ± 1.71 μM)	2.20 ± 1.25 (2.58 ± 1.46 μM)	30.16 ± 1.37 (35.32 ± 1.60 μM)	15.29 ± 0.98 (17.90 ± 1.15 μM)
Cisplatin	41.09 ± 1.30 (136.5 ± 4.32 μM)	18.00 ± 1.08 (59.78 ± 3.59 μM)	4.32 ± 1.93 (14.35 ± 6.41 μM)	3.03 ± 1.72 (10.06 ± 5.71 μM)	25.87 ± 1.02 (85.9 ± 3.39 μM)	15.35 ± 1.19 (50.98 ± 3.95 μM)

Table 2. IC₅₀ values of the synthetic compounds against SW-872 and MCF-7 as cancerous cell line and HFF-2 as a normal cell line.

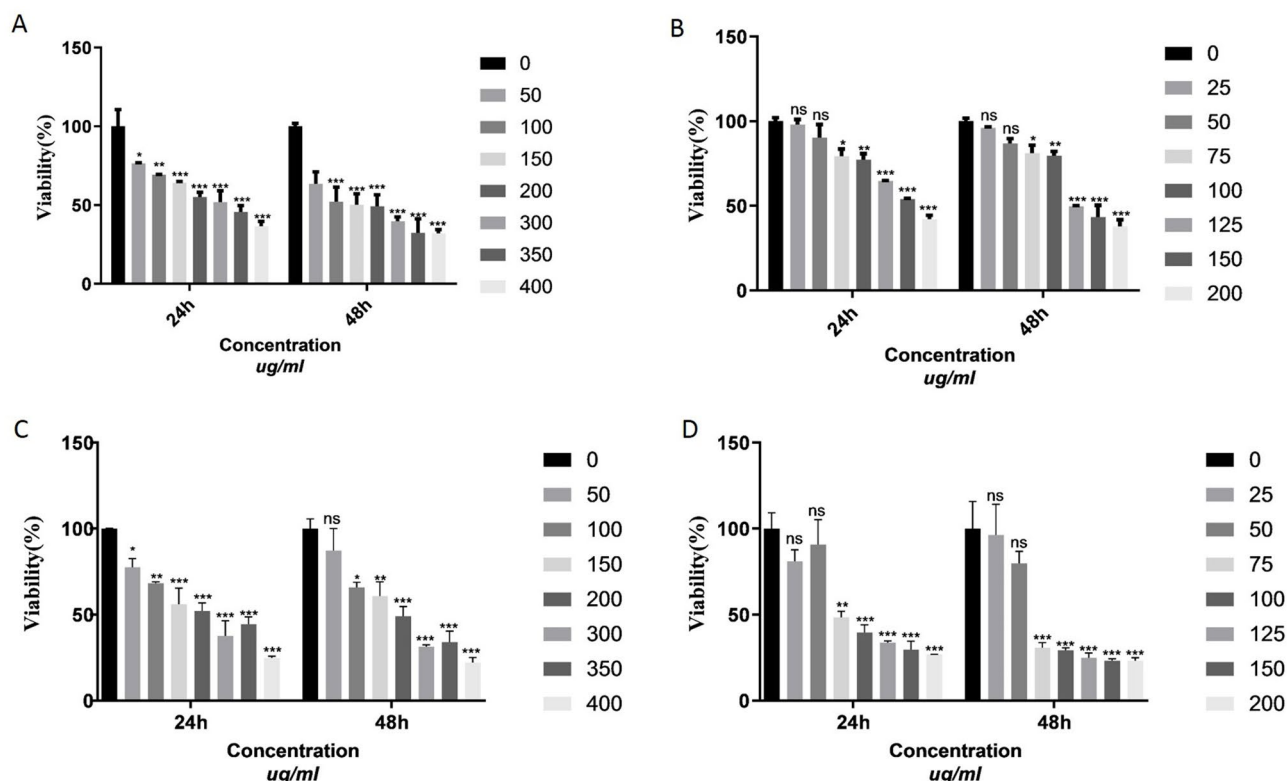


Fig. 8. Cell viability of (A) SW-872 cancer cells after treatment with L^{Mn} for 24 and 48 h, (B) SW-872 cancer cells after treatment with L^{Zn} for 24 and 48 h, (C) HFF-2 normal cells after treatment with L^{Mn} for 24 and 48 h, (D) HFF-2 normal cells after treatment with L^{Zn} for 24 and 48 h. * indicate a significant difference compared to the control group (*P value < 0.05, **P value < 0.01, ***P value < 0.001).

more efficiently reach their targets. In the context of drug design and pharmacology, both lipophilicity and water solubility play significant roles in determining cytotoxicity, but they influence it in different ways and to varying degrees. Lipophilicity is generally effective in determining a compound's ability to penetrate cell membranes and reach intracellular targets, which can then trigger cytotoxicity. However, water solubility is also crucial for ensuring the compound can be properly delivered to the target site and distributed within the body. Complexes L^{Mn} and L^{Zn} exhibit the lowest lipophilicity and the highest solubility in water among the tested complexes. It appears that while they are highly soluble in water, their lipophilicity is overshadowed by their solubility, ultimately increasing the cytotoxicity of these two complexes against cancer cells.

Cell apoptosis assay

The process of physiological cell death is identified as apoptosis, which is caused to the removal of old, damaged, and harmful cells under normal conditions and is essential for tissue development and hemostasis. In contrast, necrosis is another type of cell death that occurs because of environmental factors. Any abnormality in the process of apoptosis leads to a disorder. Cell death through apoptosis is momentous in terms of biologically and due to this point, tracking and evaluating the amount of apoptosis is very important in clinical trials. Chemotherapy drugs induce apoptosis in cancerous cells and cause to killing them⁴². There are several techniques for diagnosing apoptosis, one of them is flow cytometry. Evaluation of apoptosis is assessed by annexin V-FITC/PI staining based on cell membrane changes made. For this purpose, the L^{Zn} complex was selected. To determine the morphology of cell death, SW-872 cancer cells were treated with an IC_{25} concentration of L^{Zn} complex for 18 h. According to Fig. 9a, the major cell population showed primary apoptosis at early and then late apoptosis.

Cell cycle arrest

SW-872 cells were exposed to IC_{25} concentration of L^{Zn} complex for 18 h. The effect of the mentioned compound on the cell cycle distribution of the target cells was investigated by flow cytometry using DAPI staining. Flow cytometry consequence was reported in Fig. 9b. L^{Zn} caused an increasing population is observed in the S phase, which has increased from 12.46 to 32.94 compared to the control, and indicates that L^{Zn} causes cell cycle arrest in the S phase.

Thiosemicarbazone derivatives demonstrate antiproliferative activities against cancer cell lines through various mechanisms related to biological activities. These compounds can also influence cell cycle progression. These action mechanisms include the inhibition of ribonucleotide reductase (RNR) and topoisomerase II, the generation of reactive oxygen species (ROS), and changes to mitochondrial homeostasis. Ribonucleotide reductase is a type of metalloenzyme that is an important factor involved in the synthesis of DNA and the repair of DNA damage. It is often overexpressed in many cancer cells, making it an appealing target for researchers aiming to develop therapy.

Several thiosemicarbazones act by inhibiting the small subunit of ribonucleotide reductase. In a study, the association between the inhibition of cell proliferation and cell cycle arrest by three complexes $[Ni(tcitr)_2]$, $[Cu(tcitr)_2]$, and $[Pt(tcitr)_2]$ against a leukemia cell line (U973) was assessed. Their results showed that $[Ni(tcitr)_2]$ and $[Pt(tcitr)_2]$ induce cell cycle arrest in G2/M and S phases, respectively. In contrast, $[Cu(tcitr)_2]$ doesn't affect the cell cycle. As a potential target for the mentioned compounds, transcriptional modulation of ribonucleotide reductase (RNR) enzyme subunits was investigated. Studies on complex $[Ni(tcitr)_2]$ have shown that it causes significant modulation of different subunits of ribonucleotide reductase in cells U973. Increased expression of RRM2 indicates that this complex specifically targets this subunit of the enzyme. This complex does not affect p53 expression and acts by a p53-independent mechanism, arresting cell cycle progression and inducing apoptosis through a p53-independent mechanism. There were no changes in mRNA levels of ATR and ATM, but Chk1 and Chk2, as DNA damage sensors, were significantly expressed.

The $[Cu(tcitr)_2]$ complex was unable to induce cell cycle arrest but caused significant DNA damage. Since the activation of transcriptional profiles ATR and ATM was not observed, it is assumed that DNA damage did not occur through the DDR pathway. However, the expression of Chk1 was increased. It suggests that the mechanism of action of $[Cu(tcitr)_2]$ can be through the excessive production of ROS species, which causes interaction with DNA and damage to it.

The $[Pt(tcitr)_2]$ complex also caused severe DNA damage. Like $[Cu(tcitr)_2]$ complex, transcription of ATR and ATM was not detected, while expression of Chk2 was increased. Chk2 is directly involved in cell cycle arrest in G1-S phase⁴³.

Moreover, two thiosemicarbazones from DpT class, including DpC and Dp44mT, have been extensively studied by researchers under both in vitro and in vivo conditions. The mechanism of Dp44mT action involves its chelation to Fe and Cu metal centers in lysosomes. This process leads to the formation of active redox complexes that induce apoptosis via producing cytotoxic reactive oxygen (ROS) species, causing lysosome permeability. Evidence elucidates that these agents reduce the activity of key carcinogenic tyrosines, including EGFR, c-Met, HER2, and others. Both DpC and Dp44mT remarkably suppress the activity of various pro-carcinogenic signaling pathways in these tyrosine kinases. These pathways include AKT, RAS, STAT3, Wnt, TGF, as well as autophagic pathways. These two agents also inhibit proliferation, migration, metastasis, etc⁴⁴.

According to our result, cell cycle arrest was observed during the S phase in treated SW-872 cells with L^{Zn} . The S phase begins with DNA synthesis and concludes when all chromosomes have been replicated. During this phase, the amount of DNA in the cell doubles, while the rate of RNA transcription and protein synthesis decreases. The only exception to this trend is the increased production of histones. Several hypotheses have been proposed regarding the mechanism of cell cycle arrest in the S phase based on conducted studies: (1) The direct interaction between L^{Zn} and the DNA backbone induces DNA damage. (2) The interaction between L^{Zn} and histones leads to structural changes in chromatin. (3) By producing ROS species. (4) By inhibiting the small subunit of ribonucleotide reductase.

Live intracellular imaging by fluorescent microscope

The images obtained from the fluorescent microscope are shown in Fig. 10. The comparison of the images exhibits that with the enhancement of both concentration and treatment time, the absorption of compounds in the cells increases. Also, the distribution of substances in the cytoplasm of the cell is observed, and the increased treatment time of the cells with the mentioned compounds caused the distribution of the compounds to tend toward the cell nucleus.

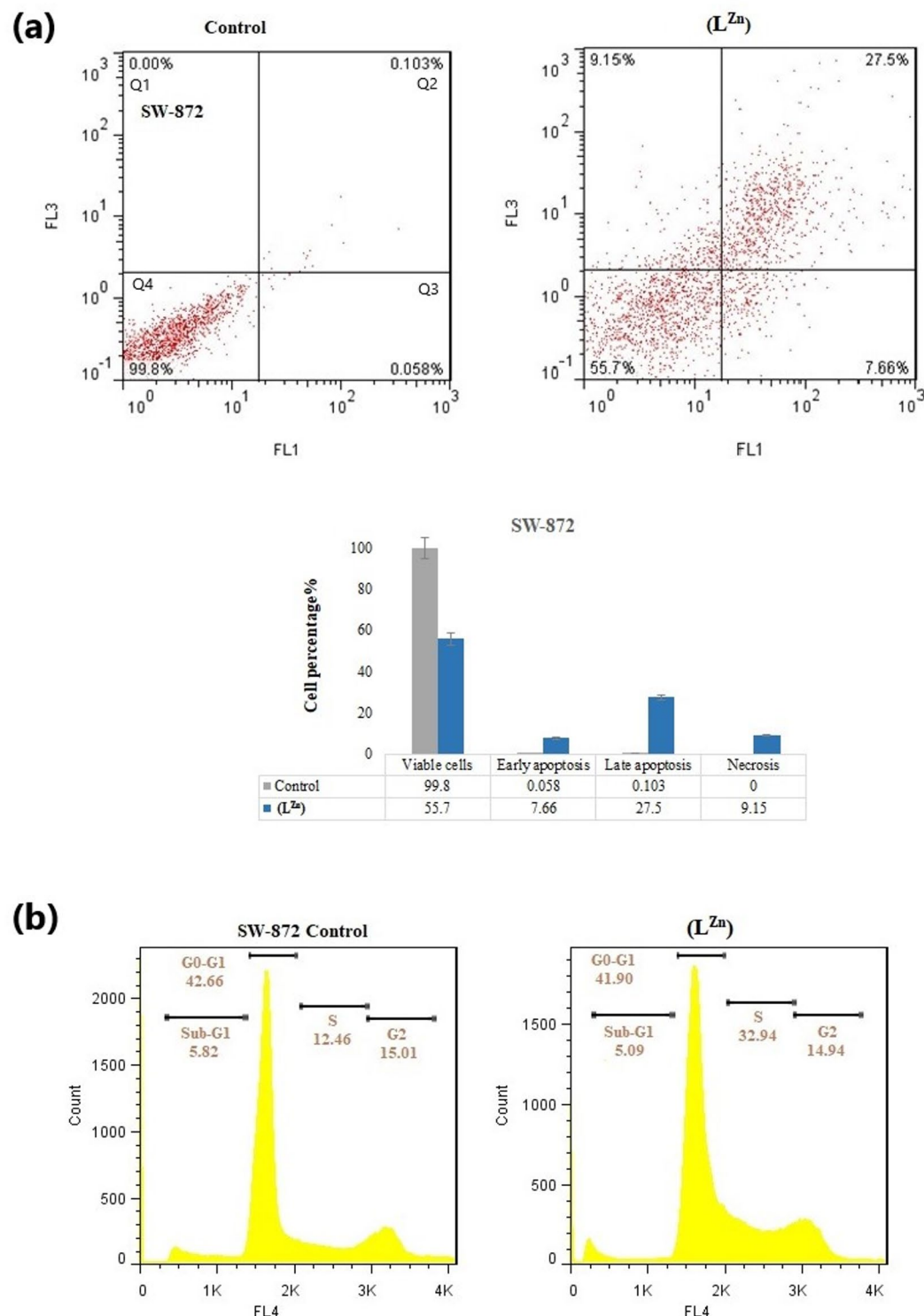


Fig. 9. (a) Evaluation of apoptosis induced by L^{Zn} against SW-872 cell line using Annexin V-FITC/PI staining based on cell membrane change, Q1: necrosis, Q2: late apoptosis, Q3: early apoptosis, Q4: viable cells. (b) Cell cycle distribution of SW-872 cells treated with IC₂₅ concentration of L^{Zn} after 18 h by flow cytometry using DAPI staining. L^{Zn} causes cell cycle arrest in the S phase.

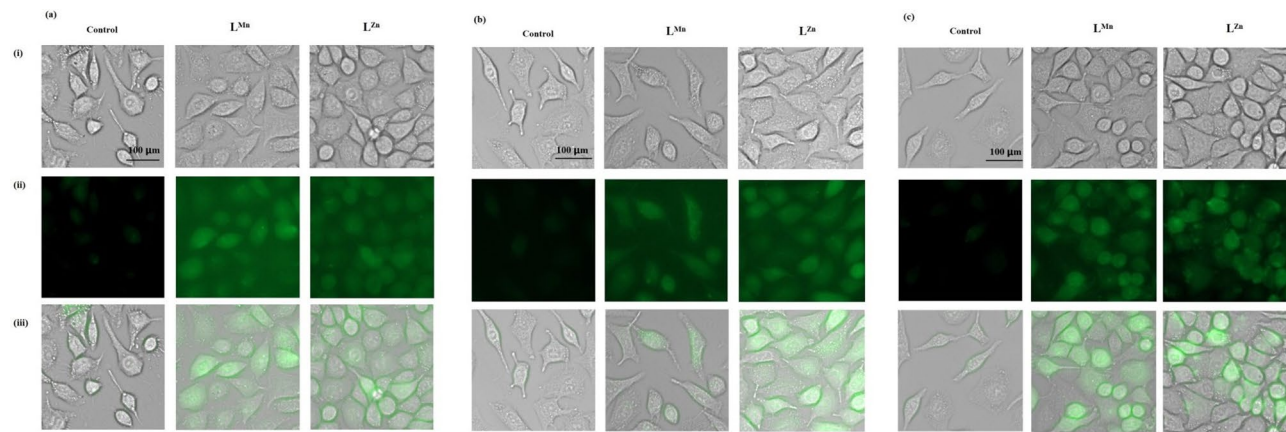


Fig. 10. The microscopy images of living MCF-7 cells treated with L^{Mn} and L^{Zn} . **(a)** Exposure to 10 μM aqueous solution of L^{Mn} and L^{Zn} for 1 h **(b)** Exposure to 100 μM aqueous solution of L^{Mn} and L^{Zn} for 1 h **(c)** Exposure to 100 μM aqueous solution of L^{Mn} and L^{Zn} for 4 h (i: bright field image, ii: fluorescent image, iii: merge of bright field and fluorescent image, Scale bar: 100 μm).

Conclusion

In the present study, a novel water-soluble fluorescent ligand containing two hydrophilic and fluorescent moieties was synthesized and identified. In order to investigate the coordination behavior of this ligand, some transition metal complexes of it were prepared. The synthesized compounds show good solubility in water. Moreover, all compounds exhibited significant stability in water solutions for 72 h or more. The toxicity of the ligand and its complexes against two cancer cell lines, MCF-7 and SW-872 was experimented by MTT assay. The compounds cleared poor inhibition against the MCF-7 cell line, while L^{Mn} and L^{Zn} complexes showed good anti-proliferative activity on SW-872 cells. Also, the toxicity of the compounds against HFF-2 normal cells in comparison with PTX (paclitaxel) and cisplatin as commercial drugs was low. L^{Zn} complex was selected as a candidate for cell apoptosis and cell cycle studies. Flow cytometry analysis confirmed that most cell death occurs through apoptosis and L^{Zn} causes cell cycle arrest in the S phase. Eventually, imaging of treated living cells via inherent fluorescence emission was performed by an immunofluorescence microscope. The increasing of both concentration and treatment time causes the absorption of compounds and the tendency toward the cell nucleus in the cells increases. However, L^{Mn} indicates almost similar anti-proliferative activity (comparable IC_{50} value ($\mu\text{g/mL}$) after 48 h treatment) to L^{Zn} against SW-872 cancerous cells. Still, it demonstrates less cytotoxicity on HFF-2 as a normal cell line compared to L^{Zn} . Therefore, the L^{Mn} complex could be a promising candidate for investigating other anticancer trials in the future, due to its lower cytotoxicity towards normal cells. A schematic diagram including the main experiments and findings of this study is shown in Fig. 11.

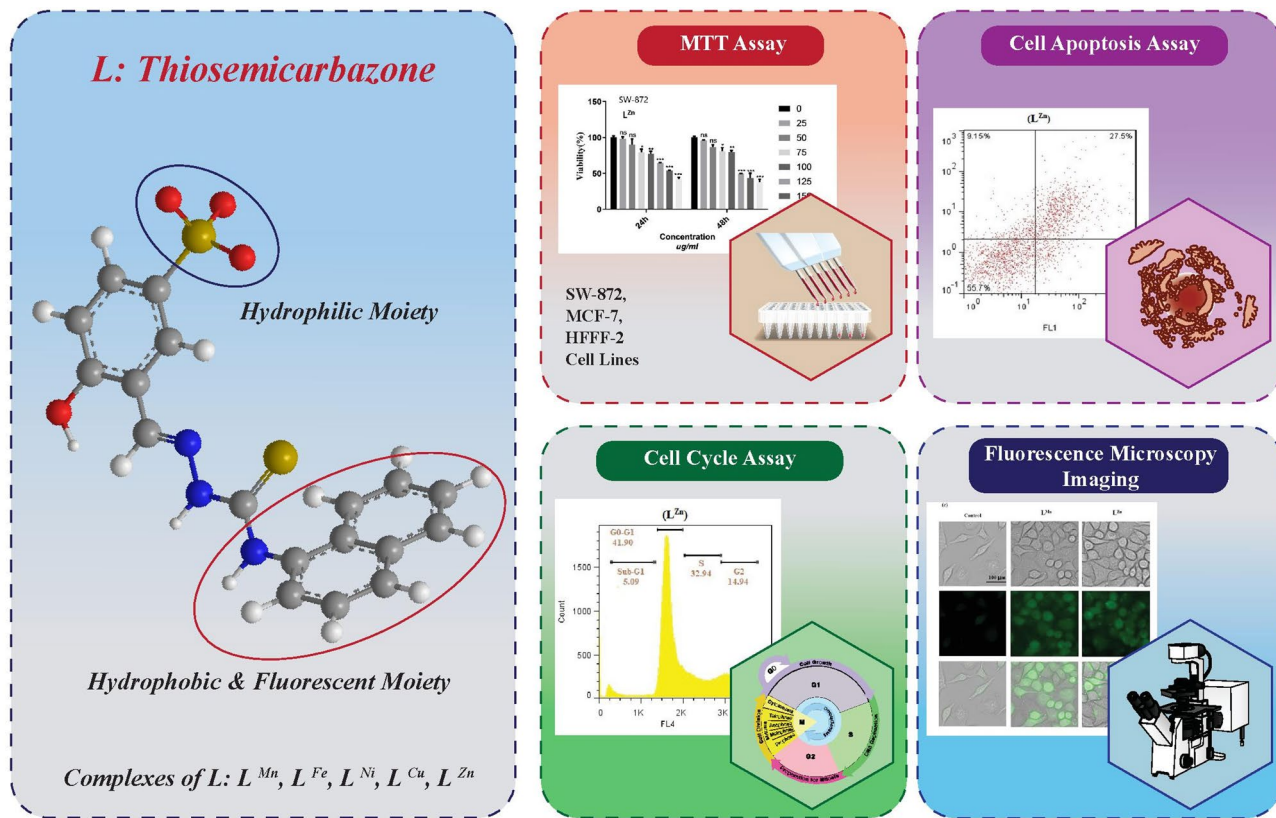


Fig. 11. Schematic of the prominent experiments and achievements.

Data availability

The data that support the findings of this study are available within the paper and its Supplementary Information. The other ones that not openly available due to reasons of sensitivity are available from the corresponding author upon reasonable request.

Received: 13 May 2025; Accepted: 23 December 2025

Published online: 26 December 2025

References

1. Kaushal, M. et al. Synthesis of 2-acetylpyridine-N-substituted thiosemicarbazones of copper (II) with high antimicrobial activity against methicillin resistant *S. aureus*, *K. pneumoniae* 1 and *C. albicans*. *New J. Chem.* **43**, 11727–11742 (2019).
2. Zaltariov, M. F. et al. New iminodiacetate-thiosemicarbazone hybrids and their copper (II) complexes are potential ribonucleotide reductase R2 inhibitors with high antiproliferative activity. *Inorg. Chem.* **56**, 3532–3549 (2017).
3. Song, J. et al. Exploring the interaction between calf thymus DNA and 11H-Indeno [1, 2-b] quinolin-11-one thiosemicarbazones: spectroscopies and in vitro antitumor activity. *Int. J. Biol. Macromol.* **295**, 139501 (2025).
4. Kaya, B. et al. Isosteric replacement of sulfur to selenium in a thiosemicarbazone: promotion of Zn (II) complex dissociation and transmetalation to augment anticancer efficacy. *J. Med. Chem.* **67**, 12155–12183 (2024).
5. Miglioli, F. et al. Anticancer activity of new water-soluble sulfonated thiosemicarbazone copper (II) complexes targeting disulfide isomerase. *Eur. J. Med. Chem.* **276**, 116697 (2024).
6. Besleaga, I. et al. Triapine analogues and their copper (II) complexes: Synthesis, characterization, solution speciation, redox activity, cytotoxicity, and mR2 RNR Inhibition. *Inorg. Chem.* **60**, 11297–11319 (2021).
7. Oliveira, A. P. et al. Triethylphosphinegold (i) complexes with secnidazole-derived thiosemicarbazones: cytotoxic activity against hct-116 colorectal cancer cells under hypoxia conditions. *ACS Omega*. **5**, 2939–2946 (2020).
8. Palamarciuc, O. et al. Investigation of the cytotoxic potential of Methyl imidazole-derived thiosemicarbazones and their copper (ii) complexes with Dichloroacetate as a co-ligand. *New J. Chem.* **43**, 1340–1357 (2019).
9. Kaya, B. et al. Structural analysis and biological functionalities of iron (III)–and manganese (III)–thiosemicarbazone complexes: in vitro anti-proliferative activity on human cancer cells, DNA binding and cleavage studies. *J. Biol. Inorg. Chem.* **24**, 365–376 (2019).
10. Wijesinghe, T. P. et al. Steric Blockade of Oxy-Myoglobin oxidation by thiosemicarbazones: Structure–Activity relationships of the novel PPP4pT series. *J. Med. Chem.* **66**, 15453–15476 (2023).
11. Qi, J., Qian, K., Tian, L., Cheng, Z. & Wang, Y. Gallium (iii)–2-benzoylpyridine-thiosemicarbazone complexes promote apoptosis through Ca²⁺ signaling and ROS-mediated mitochondrial pathways. *New J. Chem.* **42**, 10226–10233 (2018).
12. Shao, M. et al. In vitro and in vivo of triphenylamine-appended fluorescent half-sandwich iridium (III) thiosemicarbazones antitumor complexes. *Inorg. Chem.* **60**, 17063–17073 (2021).
13. Li, A. et al. Thiosemicarbazone mixed-valence Cu (I/II) complex against lung adenocarcinoma cells through multiple pathways involving Cuproptosis. *J. Med. Chem.* **67**, 9091–9103 (2024).
14. Harababu, J. et al. Synthesis of palladium (II) complexes via Michael addition: antiproliferative effects through ROS-mediated mitochondrial apoptosis and Docking with SARS-CoV-2. *Inorg. Chem.* **59**, 17109–17122 (2020).

15. Aguirre, A. R. & Bernaldo, H. The Pharmacological profile of metal complexes with Bis (thiosemicarbazones) and Bis (hydrazone)-derived ligands. *Polyhedron* **116993** (2024).
16. Vadakkedathu Palakkeezhillam, V. N. et al. Unraveling the anticancer efficacy and biomolecular properties of Ru (II)-Arene complexes of Pyrene-Based thiosemicarbazone ligands: A comprehensive in Silico/In vitro exploration. *Organometallics* **43**, 242–260 (2024).
17. Chaudhary, U. et al. Synthesis of 5-hydroxyisatin thiosemicarbazones, spectroscopic investigation, protein-ligand docking, and in vitro anticancer activity. *Bioorg. Chem.* **153**, 107872 (2024).
18. Singh, V., Haribabu, J., Moraga, D., Santibanez, J. F. & Sreekanth, A. Investigation of the anticancer potential of newly synthesized N4-substituted thiosemicarbazones: in Silico and in vitro biological approaches. *J. Mol. Struct.* **1324**, 140764 (2025).
19. Chattopadhyay, T., Biswas, C., Sreekumar, S., Kiran, M. S. & Ghosh, R. Insights into the selective anticancer activity of [SnIV (L)(Cl)2 (OH2)][L=(E)-N, N-diethyl-2-(2-hydroxy-3-methoxybenzylidene) hydrazinecarbothioamide] at thiosemicarbazone appended Tin (IV) site. *Inorg. Chem. Commun.* **165**, 112525 (2024).
20. Manakkadan, V. et al. Synthesis and characterization of copper (II) complex derived from newly synthesized Acenaphthene Quinone thiosemicarbazone ligands: computational studies, in vitro binding with DNA/BSA and anticancer studies. *Inorg. Chim. Acta.* **574**, 122369 (2025).
21. de Siqueira, L. R. P., de Moraes Gomes, P. A. T., de Lima Ferreira, L. P., de Melo Rêgo, M. J. B. & Leite, A. C. L. Multi-target compounds acting in cancer progression: focus on thiosemicarbazone, thiazole and Thiazolidinone analogues. *Eur. J. Med. Chem.* **170**, 237–260 (2019).
22. Sarkar, S. et al. A multi-responsive thiosemicarbazone-based probe for detection and discrimination of group 12 metal ions and its application in logic gates. *New J. Chem.* **42**, 15157–15169 (2018).
23. Zou, B. Q. et al. Three novel transition metal complexes of 6-methyl-2-oxo-quinoline-3-carbaldehyde thiosemicarbazone: synthesis, crystal structure, cytotoxicity, and mechanism of action. *RSC Adv.* **7**, 17923–17933 (2017).
24. Aftab, H. et al. Synthesis, in vitro biological evaluation and in Silico studies of novel pyrrolidine derived thiosemicarbazones as dihydrofolate reductase inhibitors. *RSC Adv.* **14**, 31409–31421 (2024).
25. Yu, P. et al. Anticancer and biological properties of a Zn-2, 6-diacetylpyridine Bis (thiosemicarbazone) complex. *Metallomics* **11**, 1372–1386 (2019).
26. Fang, Y., Li, J., Han, P. P., Han, Q. X. & Li, M. X. Less toxic zinc (II), Diorganotin (IV), gallium (III) and cadmium (II) complexes derived from 2-benzoylepyridine N, N-dimethylthiosemicarbazone: synthesis, crystal structures, cytotoxicity and investigations of mechanisms of action. *Toxicol. Res.* **7**, 987–993 (2018).
27. Manakkadan, V. et al. Exploring the biological efficacy of Zn (II)-Thiosemicarbazone-Ferrocene complexes: In-Silico and In-Vitro findings. *J. Inorg. Organomet. Polym. Mater.* 1–18 (2025).
28. Li, M. X., Chen, C. L., Zhang, D., Niu, J. Y. & Ji, B. S. Mn (II), Co (II) and Zn (II) complexes with heterocyclic substituted thiosemicarbazones: Synthesis, characterization, X-ray crystal structures and antitumor comparison. *Eur. J. Med. Chem.* **45**, 3169–3177 (2010).
29. Dimiza, F., Raptopoulou, C. P., Pscharis, V., Papadopoulos, A. N. & Psomas, G. Manganese (II) complexes with the non-steroidal anti-inflammatory drugs Naproxen and mefenamic acid: Synthesis, structure, antioxidant capacity, and interaction with albumins and DNA. *New J. Chem.* **42**, 16666–16681 (2018).
30. Zampakou, M. et al. Structure, antimicrobial activity, albumin-and DNA-binding of manganese (II)-sparfloxacinato complexes. *RSC Adv.* **5**, 11861–11872 (2015).
31. Hosseini-Yazdi, S. A. et al. Reactions of copper (II), nickel (II), and zinc (II) acetates with a new water-soluble 4-phenylthiosemicarbazone schiff base ligand: Synthesis, characterization, unexpected cyclization, antimicrobial, antioxidant, and anticancer activities. *Polyhedron* **124**, 156–165 (2017).
32. Hosseini-Yazdi, S. A. et al. Synthesis, characterization and in vitro biological activities of new water-soluble copper (II), zinc (II), and nickel (II) complexes with sulfonato-substituted schiff base ligand. *Inorg. Chim. Acta.* **458**, 171–180 (2017).
33. Hosseini-Yazdi, S. A. et al. Copper, nickel and zinc complexes of a new water-soluble thiosemicarbazone ligand: Synthesis, characterization, stability and biological evaluation. *J. Mol. Liq.* **248**, 658–667 (2017).
34. Mirzaahmadi, A. et al. Apoptotic induction in K562 cell line by new water-soluble complexes of nickel (II) and zinc (II). *Polyhedron* **202**, 115205 (2021).
35. Berkehile, J. & Fries, A. H. Preparation of ANTU (a-naphthylthiourea) from naphthalene. *J. Chem. Educ.* **25**, 617 (1948).
36. Cymerman-Craig, J., Moyle, M. & White, R. A. α -naphthyl isothiocyanate. *Org. Synth.* **36**, 56. <https://doi.org/10.15227/orgsyn.036.0056> (1956).
37. Li, Z., Xiang, Y. & Tong, A. Ratiometric chemosensor for fluorescent determination of Zn2+ in aqueous ethanol. *Anal. Chim. Acta.* **619**, 75–80 (2008).
38. Basu, A., Thiagarajan, D., Kar, C., Ramesh, A. & Das, G. Synthesis, crystal structure and bio-macromolecular interaction studies of pyridine-based thiosemicarbazone and its Ni (II) and Cu (II) complexes. *RSC Adv.* **3**, 14088–14098 (2013).
39. Samanta, S., Manna, U., Ray, T. & Das, G. An aggregation-induced emission (AIE) active probe for multiple targets: a fluorescent sensor for Zn 2+ and al 3+ & a colorimetric sensor for Cu 2+ and F-. *Dalton Trans.* **44**, 18902–18910 (2015).
40. Qiu, K. et al. Biscyclometalated iridium (III) complexes target mitochondria or lysosomes by regulating the lipophilicity of the main ligands. *Dalton Trans.* **45**, 16144–16147 (2016).
41. Spooner, M. J. & Gale, P. A. Anion transport across varying lipid membranes—the effect of lipophilicity. *Chem. Commun.* **51**, 4883–4886 (2015).
42. Ichim, G. & Tait, S. W. A fate worse than death: apoptosis as an oncogenic process. *Nat. Rev. Cancer.* **16**, 539–548 (2016).
43. Montalbano, S., Bisceglie, F., Pelosi, G., Lazzaretti, M. & Buschini, A. Modulation of transcription profile induced by antiproliferative thiosemicarbazone metal complexes in U937 cancer cells. *Pharmaceutics* **15**, 1325 (2023).
44. Paukovcova, S. et al. Novel thiosemicarbazones sensitize pediatric solid tumor cell-types to conventional chemotherapeutics through multiple molecular mechanisms. *Cancers* **12**, 3781 (2020).

Acknowledgements

This project was financially supported by University of Tabriz and Iran National Science (INSF). The authors gratefully acknowledge Ardabil University of Medical Sciences and Immunology Research Center of Tabriz University of Medical Sciences. Also, the authors wish to acknowledge the Prof. Behzad Baradaran for their advice and efforts.

Author contributions

Seyed Abolfazl Hosseini-Yazdi, Sima Feizpour, and Elham Safarzadeh conceived and planned the study; Sima Feizpour carried out the experiment and collected available literature; Behzad Baradaran and Farhad Eslami provided some necessary equipment; Sima Feizpour, Seyed Abolfazl Hosseini-Yazdi, and Elham Safarzadeh prepared the manuscript, analyzed the statistical data, and verified the accuracy of the tests.

Funding

This project was financially supported by University of Tabriz and Iran National Science (INSF).

Declarations

Competing interests

The authors declare no competing interests.

Additional information

Supplementary Information The online version contains supplementary material available at <https://doi.org/10.1038/s41598-025-33889-5>.

Correspondence and requests for materials should be addressed to S.A.H.-Y. or E.S.

Reprints and permissions information is available at www.nature.com/reprints.

Publisher's note Springer Nature remains neutral with regard to jurisdictional claims in published maps and institutional affiliations.

Open Access This article is licensed under a Creative Commons Attribution-NonCommercial-NoDerivatives 4.0 International License, which permits any non-commercial use, sharing, distribution and reproduction in any medium or format, as long as you give appropriate credit to the original author(s) and the source, provide a link to the Creative Commons licence, and indicate if you modified the licensed material. You do not have permission under this licence to share adapted material derived from this article or parts of it. The images or other third party material in this article are included in the article's Creative Commons licence, unless indicated otherwise in a credit line to the material. If material is not included in the article's Creative Commons licence and your intended use is not permitted by statutory regulation or exceeds the permitted use, you will need to obtain permission directly from the copyright holder. To view a copy of this licence, visit <http://creativecommons.org/licenses/by-nc-nd/4.0/>.

© The Author(s) 2025